Thermodynamic Analysis of Black Holes with Multiple Horizons in Beyond Horndeski Gravity

Yun Soo Myung *

Posted Date: 28 January 2026

doi: 10.20944/preprints202601.2185.v1

Keywords: beyond Horndeski gravity; hairy black holes; thermodynamics of black holes

 doi:10.20944/preprints202601.2185.v1

Article

Thermodynamic Analysis of Black Holes with Multiple Horizons in Beyond Horndeski Gravity

Yun Soo Myung

Center for Quantum Spacetime, Sogang University, Seoul 04107, Republic of Korea; ysmyung@inje.ac.kr

Abstract

We perform thermodynamic analysis of primary and secondary hair black holes found in Beyond Horndeski gravity. It turns out that even though the strong energy condition is violated for primary hair black hole, it is a singular black hole. The primary hair black hole is described completely by three parameters of mass M, action parameter λ, and $\xi = \eta q^5$ (action parameter η and scalar charge q). We choose three cases of $\xi = 243, 5.51, 0.219$ to represent primary hair black hole properly. Four horizons with $\xi = 243$ make a closed loop in the horizon space. The secondary hair black hole depends on M and λ which becomes a magnetic charge in connection with the regular (Bardeen) black hole. We observe that the action parameter λ plays an important role in describing primary and secondary hair black holes. It is shown that the secondary hair black hole may transit into the primary hair black hole when analyzing heat capacity and Gibbs free energy. However, for two double horizons with ξ=5.51 and 0.219 forming closed loops, their thermodynamic descriptions are quite different from four horizons and thus, they could represent a new feature of primary hair black hole. Finally, the shadow radius analysis is performed to distinguish four horizons from two double horizons by comparing them with the EHT observation.

Keywords: beyond Horndeski gravity; hairy black holes; thermodynamics of black holes

1. Introduction

Comments:

Horndeski gravity [1] was believed to be the most general scalar-tensor gravities of avoiding Ostrogradsky instabilities. However, recent achievements [2–8] allowed for the Beyond Horndeski as well as Degenerate Higher Order Scalar Tensor (DHOST) classifications.

The primary hair black holes could be found from a linear time dependence in the ansatz of the scalar field $\Phi = qt + \Psi(r)$, which is permitted by the shift symmetry of the Beyond Horndeski action, whereas the staticity of the metric remains unaffected [9–11]. The primary scalar hair charge q can be understood as the physical attribute which differs from the mass, electric charge, angular momentum of the black hole, action parameters and thus, it compares to the secondary scalar hair. However, the study on the thermal properties of these black holes have remained unclear for a long time [12].

Recently, the black hole solutions with primary scalar hair were obtained from the shift and parity symmetric subclass of Beyond Horndeski gravities [13–15]. These solutions depend on the mass M and scalar charge q, in addition to two action parameters η and λ. For a choice of $\eta q^5 (\equiv \xi) = 3\sqrt{2}M/\lambda$, it reduces to the regular (Bardeen) black hole solution described by mass M and magnetic charge λ with secondary scalar hair. More recently, the thermodynamic formalism of primary hair black hole was achieved and it was compared to the regular black hole with secondary hair [16]. Thermodynamic and observational constraints on other type of primary hairy black holes appeared in [17].

On the other hand, the spontaneous scalarization of Bardeen black hole was performed in the Einstein-nonlinear electrodynamic theory by considering quadratic $(1 - \alpha\varphi^2)$ and exponential $(e^{-\alpha\varphi^2})$ coupling functions [18]. It is worth noting that this scalarization was triggered by tachyonic instability of Bardeen black hole without scalar hair. In this case, infinite branches $(n = 0, 1, 2, \cdots)$ of scalarized

 doi:10.20944/preprints202601.2185.v1

charged black holes with primary scalar hair were constructed numerically, whereas the $n = 0$ branch is stable against radial perturbation. This is the same as Reissner-Nordström (RN) black hole in the Einstein-Maxwell-scalar theory [19–21].

In this study, we wish to perform an explicitly thermodynamic analysis of two black holes with primary and secondary hairs found in Beyond Horndeski gravity. We will show that primary hair black hole with three parameters of (M, λ, ξ) is singular even though the strong energy condition is violated for $r < \sqrt{2/3}\lambda$ in the tangential pressures p_θ and $\hat{p}_\theta$. However, the primary hair solution has a complicated horizon structure inspired by its metric function $h(r)$ in Equation (4). Therefore, one should select ξ to represent the primary black hole appropriately. Here, we will choose three special cases of ξ=243 for four horizons and ξ=5.51 and 0.219 for two double horizons to study thermodynamics of primary hair black hole. It is interesting to note that the primary hair black hole has four horizons for $0 < \lambda < 0.0192$ and the secondary hair black hole has double horizons for $0 < \lambda < 0.7698$. Therefore, they violate no scalar-haired inner horizon theorem which states that there is no inner horizon if static black holes have with non-trivial scalar hairs [22–25]. Hence, these two black holes may be regarded as counter examples to no scalar-haired inner horizon theorem.

The present work will include computing all thermodynamic quantities with the area-law entropy, checking the first law thermodynamics and the Smarr formula, and studying a phase transition between two black holes by taking into account heat capacity and Gibbs free energy. Our analysis is important to understand similarity and difference between two black holes with primary and secondary hairs. On the other hand, for the primary hair black hole of two double horizons with $0 < \lambda < 0.7694$ and $0 < \lambda < 19.4$, their thermodynamic properties are different from four horizons and thus, these represent a new feature of primary hair black hole. Finally, we perform the shadow radius analysis to distinguish four horizons from two double horizons.

2. Beyond Horndeski Gravity and Its Solutions

We introduce the Beyond Horndeski gravity action which respects both shift and parity symmetry with $c = G = 1$ as

$$S_{\rm BHG} = \frac{1}{16\pi}\int d^4x\sqrt{-g}\Big[G_4(X)R \quad + \quad G_{4X}(X)[(\Box\Phi)^2 - \Phi_{;\mu\nu}\Phi^{;\mu\nu}] \\ + \quad G_2(X) + F_4(X)\epsilon^{\mu\nu\rho\sigma}\epsilon^{\alpha\beta\gamma}{}_{\sigma}\Phi_{;\mu}\Phi_{;\alpha}\Phi_{;\nu\beta}\Phi_{;\rho\gamma}\Big]. \tag{1}$$

Here, $G_4(X)$, $G_2(X)$, and $F_4(X)$ are arbitrary functions of $X = -\partial^\mu\Phi\partial_\mu\Phi/2$, the derivatives of the scalar field is defined as $\Phi_{;\mu\nu} \equiv \nabla_\mu\partial_\nu\Phi$, and a subscript X denotes derivative with respect to X. The inclusion of F_4-term represents Beyond Horndeski gravity. Concerning the scalar field, we choose

$$\Phi(t, r) = qt + \Psi(r)\,, \tag{2}$$

where the linear time dependence is allowed because of the shift symmetry ($\Phi \to \Phi+$ const.) of the action.

We are interested in finding a static and homogeneous black hole solution with a primary scalar hair. For this purpose, we introduce the line element

$$ds^2 = -h(r)dt^2 + \frac{dr^2}{h(r)} + r^2 d\Omega_2^2. \tag{3}$$

 doi:10.20944/preprints202601.2185.v1

The homogeneity of the solution is supported by choosing $G_2 = -2(\eta/\lambda^2)X^{5/2}$, $G_4 = 1 - \eta X^{5/2}$, and $F_4 = \eta X^{1/2}$ [15]. In this case, the metric function is expressed in terms of four positive parameters (M, λ, η, q) as

$$h(r) = 1 - \frac{2M}{r} - \frac{\sqrt{2}\eta q^5 \lambda}{3r}\Big(\frac{r^2}{(r^2+\lambda^2)^{3/2}} - 1\Big) \equiv 1 - \frac{2m_f(r)}{r} \tag{4}$$

with a mass function $m_f(r)$ and $X = q^2\lambda^2/2(r^2+\lambda^2)$.

First of all, we wish to check that the length dimensions of parameters are given by $[M] = [\lambda] = L$, $[\eta] = L^{-5}$, and $[q] = L$. This implies that ηq^5 is a dimensionless quantity and thus, it is defined as "$\xi = \eta q^5$" to classify the primary hair black holes. As is shown in Figure 1a, one mass function $m_f(r, M = 1, \xi = 243, \lambda = 0.1)$ is -4.73 at $r = 0$ and $1(= M)$ near the outer horizon at $r \simeq 2$. The others are given by $m_f(r, 1, 5.51, 0.1)$ and $m_f(r, 1, 0.219, 0.1) \simeq 1$. The zero mass function at $r = 0$ requires $\xi = \frac{3\sqrt{2}M}{\lambda}$, being a condition for recovering the regular black hole. See Figure 1b for those functions. We stress that $\lambda = 0.01746, 0.7698, 19.4$ are found for $\xi = 243, 5.51, 0.219$, respectively. Actually, the mass functions contain all information on forming black hole spacetimes.

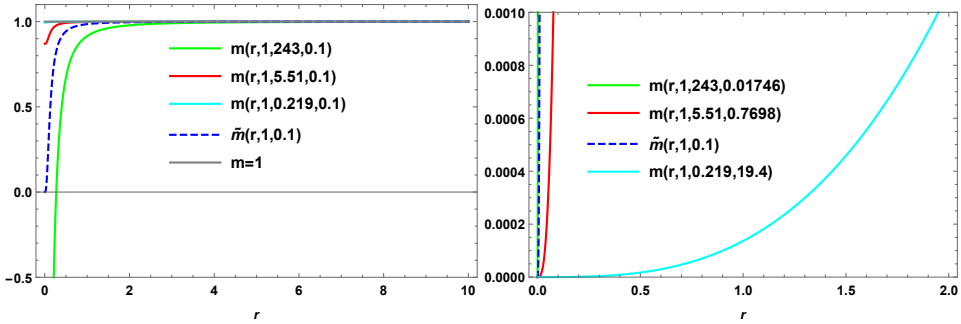

(**a**) (**b**)

Figure 1. (a) Four mass functions $m_f(r, M = 1, \xi = 243, \lambda = 0.1)$, $m_f(r, 1, 5.51, 0.1)$, $m_f(r, 1, 0.219, 0.1) \simeq 1$, and $\tilde{m}_f(r, M = 1, \lambda = 0.1)$ for secondary hair black hole as functions of r. They are different inside the outer horizon at $r \simeq 2$, while they are nearly the same outside the horizon. (b) Their zero mass functions at $r = 0$ are allowed for $\lambda(\xi) = 0.01746(243), 0.7698(5.51), 1, 19.4(0.219)$.

To see whether this solution is regular or not, we expand $h(r)$ around $r = 0$ as

$$h(r) \simeq 1 - \frac{\sqrt{2}\xi}{3\lambda^2}r^2 + \frac{\sqrt{2}(\xi\lambda - 3\sqrt{2}M)}{3r} + \cdots, \tag{5}$$

where it reduces to the de Sitter core $(1 - \frac{2Mr^2}{\lambda^3})$ if one chooses $\xi = \frac{3\sqrt{2}M}{\lambda}$, leading to the regular black hole. This shows that the primary hair black hole is singular.

From the action Equation (1), one finds the Einstein equation

$$G_4(X)G_{\mu\nu} = T_{\mu\nu} \to G_{\mu\nu} = T^{\rm eff}_{\mu\nu}, \quad T^{\rm eff}_{\mu\nu} = \frac{T_{\mu\nu}}{G_4(X)}, \tag{6}$$

 doi:10.20944/preprints202601.2185.v1

where $T_{\mu\nu}$ includes all the terms except $G_{\mu\nu}$ after varying the action with respect to $g_{\mu\nu}$. We find that the energy density ρ, radial pressure p_r, and tangential pressure p_θ are given by

$$\rho(r,\eta,\lambda,q) \equiv -T^{\text{eff},t}{}_t = -G^t{}_t = \frac{\sqrt{2}\xi\lambda^3}{(r^2+\lambda^2)^{5/2}}, \tag{7}$$

$$p_r(r,\eta,\lambda,q) \equiv T^{\text{eff},r}{}_r = G^r{}_r = -\frac{\sqrt{2}\xi\lambda^3}{(r^2+\lambda^2)^{5/2}}, \tag{8}$$

$$p_\theta(r,\eta,\lambda,q) \equiv T^{\text{eff},\theta}{}_\theta = G^\theta{}_\theta = \frac{\xi\lambda^3(3r^2-2\lambda^2)}{\sqrt{2}(r^2+\lambda^2)^{7/2}}, \tag{9}$$

which all are independent of the black hole mass M. Here, we prove that null energy condition (NEC: $\rho+p_r\geq 0$ and $\rho+p_\theta\geq 0$), weak energy condition (WEC: NEC and $\rho\geq 0$), and dominant energy condition (DEC: $\rho-p_r\geq 0$ and $\rho-p_\theta\geq 0$) are satisfied but strong energy condition (SEC: NEC and $\rho+p_r+2p_\theta\geq 0$) is violated for $r<r_{\text{SEC}}=\sqrt{2/3}\lambda=0.816\lambda$ [26]. The latter may imply that the primary hair black hole is regular, but it is surely singular as is shown in Equation (5).

On the other hand, choosing $\xi=3\sqrt{2}M/\lambda$ (or zero mass function at $r=0$) and thus, disappearing the $1/r$-term leads to the regular black hole with its mass function $\tilde{m}_f(r)$

$$f(r)=1-\frac{2Mr^2}{(r^2+\lambda^2)^{3/2}}\equiv 1-\frac{2\tilde{m}_f(r)}{r} \tag{10}$$

and its scalar derivative square

$$[\tilde{\Psi}'(r,M,\eta,\lambda)]^2=\frac{\left(\frac{3\sqrt{2}M}{\eta\lambda}\right)^{2/5}}{f^2(r)}\Big[1-\frac{f(r)}{1+(r/\lambda)^2}\Big]. \tag{11}$$

We note that the mass function $\tilde{m}_f(r,M,\lambda)$ is always zero at $r=0$ irrespective of M and λ, differing from primary hair black hole. As is shown in Figure 1a, we check that $\tilde{m}_f(r,M=1,\lambda=0.1)$ is zero at $r=0$ and $1(=M)$ near the outer horizon at $r\simeq 2$. In this case, two (outer/inner) horizons exist for $0<\lambda<4M/3\sqrt{3}$ and they shrink into an extremal black hole at $\lambda=4M/3\sqrt{3}$. However, for $\lambda>4M/3\sqrt{3}$, there is no horizon to $f(r)=0$, implying the presence of naked singularity (NS). Its energy density, radial pressure, and tangential pressure are given by

$$\tilde{\rho}(r,M,\lambda)=\frac{6M\lambda^2}{(r^2+\lambda^2)^{5/2}},\quad \tilde{p}_r(r,M,\lambda)=-\frac{6M\lambda^2}{(r^2+\lambda^2)^{5/2}},\quad \tilde{p}_\theta=\frac{3M\lambda^2(3r^2-2\lambda^2)}{(r^2+\lambda^2)^{7/2}}. \tag{12}$$

It is shown that NEC ($\tilde{\rho}+\tilde{p}_r\geq 0$, $\tilde{\rho}+\tilde{p}_\theta\geq 0$), WEC (NEC and $\tilde{\rho}\geq 0$), and DEC ($\tilde{\rho}-\tilde{p}_r\geq 0$, $\tilde{\rho}-\tilde{p}_\theta\geq 0$) are satisfied but SEC (NEC and $\tilde{\rho}+\tilde{p}_r+2\tilde{p}_\theta\geq 0$) is not satisfied for $r<r_{\text{SEC}}=\sqrt{2/3}\lambda=0.816\lambda$. The latter means that the secondary hair black hole is a regular black hole [27,28]. In this case, the region which SEC is violated is situated inside the outer horizon ($\tilde{r}_+$).

At this stage, it is interesting to note that the solution $f(r)$ in Equation (10) is the same form of the Bardeen black hole without scalar hair obtained from the Einstein-nonlinear electrodynamics action

$$S_{\text{ENE}}=\frac{1}{16\pi}\int d^4x\sqrt{-g}\Big[R-4\mathcal{L}(\mathcal{F})\Big], \tag{13}$$

where $\mathcal{L}(\mathcal{F})$ is a nonlinear function of $\mathcal{F}=F_{\mu\nu}F^{\mu\nu}/4$ defined by

$$\mathcal{L}(\mathcal{F})=\frac{3M}{|\lambda|\lambda^2}\left(\frac{\sqrt{2\lambda^2\mathcal{F}}}{1+\sqrt{2\lambda^2\mathcal{F}}}\right)^{\frac{5}{2}}. \tag{14}$$

 doi:10.20944/preprints202601.2185.v1

Here, M and λ are two parameters associated with the mass and magnetic charge of the Bardeen black hole, respectively. In this case, the Einstein equation takes the from

$$G_{\mu\nu} = \hat{T}_{\mu\nu}, \quad \hat{T}_{\mu\nu} = -2\mathcal{L}(\mathcal{F})g_{\mu\nu} + 2\frac{\partial\mathcal{L}(\mathcal{F})}{\partial\mathcal{F}}F_{\mu\rho}F_{\nu}{}^{\rho}. \tag{15}$$

Here, the magnetic field strength is expressed as

$$F_{\mu\nu} = 2\delta^{\theta}_{[\mu}\delta^{\phi}_{\nu]}\lambda\sin\theta, \tag{16}$$

implying $F_{\theta\phi} = \lambda\sin\theta$ and $\mathcal{F} = \frac{\lambda^2}{2r^4}$. Computing its energy-momentum tensor defined by $\hat{T}_{\mu}{}^{\nu} = \text{diag}[-\hat{\rho}, \hat{p}_r, \hat{p}_t, \hat{p}_t]$, one confirms that $\tilde{\rho} = \hat{\rho}$, $\tilde{p}_r = \hat{p}_r, \tilde{p}_\theta = \hat{p}_\theta$, showing a clear connection between secondary hair and Bardeen black holes. Actually, they are identical.

3. Thermodynamic Analysis

In this section, we wish to study their thermodynamics in the grand canonical ensemble. In this ensemble, the entropy S and action parameter λ change with the surrounding heat bath, while temperature and chemical potential are fixed. It is important to note that two of action parameter η and scalar charge q are irrelevant to describing thermodynamics of primary hair black hole because their product $\xi = \eta q^5$ is a dimensionless quantity. Instead, ξ will be used to classify primary hair black holes. One can choose three special cases: ξ=243 for four horizons and ξ=5.51, 0.219 for two double horizons to represent primary hair black hole appropriately. For $M = 1$, their zero mass functions at $r = 0$ appear at $\lambda = 0.01746$ inside $\lambda \in$ [0,0.7698] for Bardeen black hole, $\lambda = 0.7698$ near Bardeen Black hole, and $\lambda = 19.4$ beyond Bardeen black hole, respectively (see Figure 1b).

From $h(r) = 0$, one finds four real solutions and four complex solutions

$$r_i(M, \xi, \lambda), \text{ for } i = 1, 2, 3, 4, \tag{17}$$
$$r_j(M, \xi, \lambda), \text{ for } j = 5, 6, 7, 8, \tag{18}$$
$$\tag{19}$$

where the latter may represent point solutions if M, λ, and ξ are chosen appropriately. Interestingly, we may establish two relations for horizon between primary and secondary hair black holes: $r_{6/5}(M = 1, \xi = 3\sqrt{2}/\lambda, \lambda) = \tilde{r}_{\pm}(M = 1, \lambda)$ when imposing $\xi = 3\sqrt{2}/\lambda$. This means that secondary hair black hole can be embedded into the primary hair black hole through horizons $r_{6/5}$.

We wish to explain why we choose three cases of 243,5.51,0.219. If ξ increases from $\xi = 243$, all allowed regions λ for r_i decreases: for $\xi = 1000$, $0.002 < \lambda < 0.12$ for major $r_{4/3}$ and $0 < \lambda < 0.002$ for minor $r_{2/1}$. If ξ decreases from $x = 243$ (see Figure 2(a)), all allowed regions λ for major $r_{4/3}$ and minor $r_{2/1}$ increase until $\xi = 34$ where $r_{4/3}$ represent the largest loop for λ (see Figure 2(b)). For $33 < \lambda < 12$, r_4 is not suitable for describing the outer horizon. For $3.8 < \xi < 11$, the major outer/inner horizons are described by $r_{2/1}$. We choose $\xi = 5.51$ to represent this range (see Figure 6(a)). For $0 < \xi < 3.8$, the allowed regions λ for $r_{4/3}$ are not available but the allowed regions λ for $r_{2/1}$ increases. Finally, we choose $\xi = 0.219$ to represent this range (see Figure 7a).

 doi:10.20944/preprints202601.2185.v1

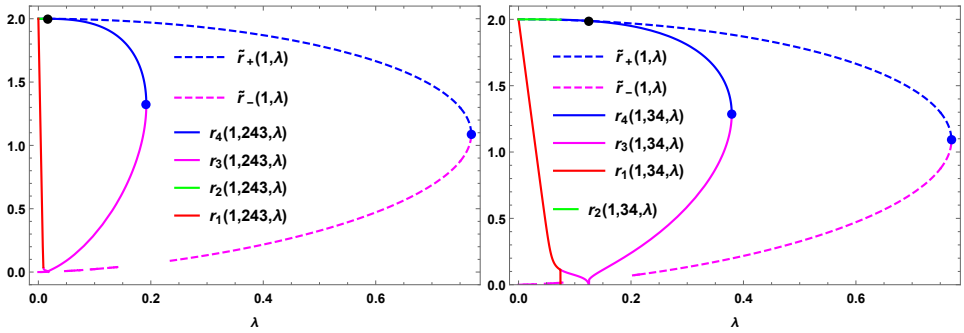

(a) (b)

Figure 2. (a) Four horizons $r_i(M=1,\xi=243,\lambda)$ with $r_6(1,243,0.01746)$ (•) showing a closed loop formed by $r_{4/3}(1,243,\lambda\in[0.009,0.192])$ and $r_{2/1}(1,243,\lambda\in[0,0.009])$, and double horizons $\tilde{r}_\pm(M=1,\lambda)$ for secondary hair black hole as function of $\lambda\in[0,0.7698]$. (b) Four horizons $r_i(1,34,\lambda)$ are functions of λ, showing the largest loop formed by $r_{4/3}(1,34,\lambda\in[0.075,0.379])$ and $r_{2/1}(1,34,\lambda\in[0,0.075])$ with $r_6(1,34,0.125)$ (•).

Now, let us study the thermodynamics of black holes with multiple horizons r_i. We find that black hole mass $m_i(=M)$ obtained from $h(r_i)=0$, the area-law entropy $S_i=\pi r_i^2$, the Hawking temperature defined by $T_i=\frac{\partial m_i}{\partial S_i}$, heat capacity $C_i=T_i\frac{\partial S_i}{\partial r_i}(\frac{\partial T_i}{\partial r_i})^{-1}$, chemical potential $W_{i\lambda}=\frac{\partial m_i}{\partial\lambda}$, and Gibbs free energy $G_i=m_i-T_iS_i-W_{i\lambda}\lambda$ as

$$m_i(M,\xi,\lambda) = \frac{r_i}{2}\Big[1+\frac{\sqrt{2}\xi\lambda}{3r_i}\Big(1-\frac{r_i^3}{(r_i^2+\lambda^2)^{3/2}}\Big)\Big], \tag{20}$$

$$T_i(M,\xi,\lambda) = \frac{-\sqrt{2}\xi\lambda^3r_i^2+(r_i^2+\lambda^2)^{5/2}}{4\pi r_i\big(r_i^2+\lambda^2\big)^{5/2}}, \tag{21}$$

$$C_i(M,\xi,\lambda) = -\frac{2\pi r_i(r_i^2+\lambda^2)[-\sqrt{2}\xi\lambda^3r_i^2+(r_i^2+\lambda^2)^{5/2}]}{\sqrt{2}\xi\lambda^3r_i^2(\lambda^2-4r_i^2)+(r_i^2+\lambda^2)^{7/2}}, \tag{22}$$

$$W_{i\lambda}(M,\xi,\lambda) = \frac{\sqrt{2}\xi}{6}\Big[1-\frac{r_i^3(r_i^2-2\lambda^2)}{(r_i^2+\lambda^2)^{5/2}}\Big], \tag{23}$$

$$G_i(M,\xi,\lambda) = \frac{r_i}{4}\Big[1-\frac{\sqrt{2}\xi\lambda^3r_i^2}{(r_i^2+\lambda^2)^{5/2}}\Big]. \tag{24}$$

We note that T_i is also derived from the surface gravity $\kappa/2\pi=h'(r)|_{r\to r_i}/4\pi$ with $M\to m_i$, while C_i can be obtained from the other definition of $(\partial m_i/\partial r_i)(\partial T_i/\partial r_i)^{-1}$.

At this stage, we wish to check that the first-law of thermodynamics is satisfied as [29]

$$dm_i=T_idS_i+W_{i\lambda}d\lambda. \tag{25}$$

Also, the Smarr formula takes the form

$$m_i=2T_iS_i+W_{i\lambda}\lambda. \tag{26}$$

Here, we stress that an action parameter λ is considered as an important thermodynamic variable [30, 31]. From observing Equations (21) and (22), T_i and C_i are zero when their numerators are zero, showing extremal points, while C_i blows up when its denominator is zero, leading to the Davies point for phase transition.

On the other hand, it is worth noting that making a simple replacement of $\xi\to 3\sqrt{2}M/\lambda$ on Equations (21)-(24) does not lead to correct thermodynamic quantities for secondary hair black

 doi:10.20944/preprints202601.2185.v1

hole. Therefore, we define the ADM mass and the area-law entropy as $\tilde{m}$ and $\tilde{S} = \pi\tilde{r}_+^2$. Then, its thermodynamic quantities are determined by [32]

$$\tilde{m}(M,\lambda) = \frac{(\tilde{r}_+^2+\lambda^2)^{3/2}}{2\tilde{r}_+^2}, \tag{27}$$

$$\tilde{T}_{\rm H}(M,\lambda) = \frac{(\tilde{r}_+^2-2\lambda^2)\sqrt{\tilde{r}_+^2+\lambda^2}}{4\pi\tilde{r}_+^4}, \tag{28}$$

$$\tilde{C}(M,\lambda) = -\frac{2\pi\tilde{r}_+^2(\tilde{r}_+^2-2\lambda^2)(\tilde{r}_+^2+\lambda^2)}{\tilde{r}_+^4-4\lambda^2\tilde{r}_+^2-8\lambda^4}, \tag{29}$$

$$\tilde{W}_\lambda(M,\lambda) = \frac{3\lambda\sqrt{\tilde{r}_+^2+\lambda^2}}{2\tilde{r}_+^2}, \tag{30}$$

$$\tilde{G}(M,\lambda) = \tilde{m}-\tilde{T}_{\rm H}\tilde{S}-\tilde{W}_\lambda\lambda = \frac{\sqrt{\tilde{r}_+^2+\lambda^2}(\tilde{r}_+^2-2\lambda^2)}{4\tilde{r}_+^2}, \tag{31}$$

where $\tilde{r}_+(M,\lambda)$ denotes the largest real root to $f(r)=0$. The location of outer horizon for secondary hair black hole given by [33]

$$\tilde{r}_+(M,\lambda) = \sqrt{\frac{1}{3}(4M^2-3\lambda^2)+\frac{2^{1/3}}{3}\chi(M,\lambda)+\frac{2^{2/3}(8M^4-12M^2\lambda^2)}{3\chi(M,\lambda)}} \tag{32}$$

with

$$\chi(M,\lambda) = \sqrt[3]{32M^6-72M^4\lambda^2+27M^2\lambda^6+3\sqrt{81M^4\lambda^8-48M^6\lambda^6}}. \tag{33}$$

One finds from the inner root of $\chi(M,\lambda)$ that the condition $0<\lambda<4\sqrt{3}M/9$ must fulfill for the existence of two (outer/inner) horizons. In the limit of $\lambda\to 4\sqrt{3}M/9$, one finds the extremal black hole. As is expected, the first-law of thermodynamics is satisfied as

$$d\tilde{m} = \tilde{T}_{\rm H}d\tilde{S}+\tilde{W}_\lambda d\lambda. \tag{34}$$

We check that the Smarr formula is satisfied as

$$\tilde{m} = 2\tilde{T}_{\rm H}\tilde{S}+\tilde{W}_\lambda\lambda. \tag{35}$$

Here, it is important to note that the temperature $[\tilde{T}_{\rm H}(M,\lambda)=\partial\tilde{m}/\partial\tilde{S}]$ is not equal to $\kappa/2\pi = f'(\tilde{r}_+)/4\pi = \frac{\tilde{r}_+^2-2\lambda^2}{4\pi\tilde{r}_+(\tilde{r}_+^2+\lambda^2)}$ derived from the surface gravity. One notes that the first-law is not satisfied with $f'(\tilde{r}_+)/4\pi$ [34]. It remains a controversial issue to define a proper temperature in the Bardeen black hole. Here, we prefer the first-law than the surface gravity to define the temperature of secondary hair black hole when choosing the area-law entropy. Observing Equations (28), (29), and (31), temperature $\tilde{T}_{\rm H}$, heat capacity $\tilde{C}$, and free energy $\tilde{G}$ are zero (extremal point) when their numerators are zero, while $\tilde{C}$ blows up (Davies point) when its denominator is zero. Finally, we mention that considering the $j=6$ case with $r_6(M,3\sqrt{2}M/\lambda,\lambda)$ in Equations (20)-(24) does not recover Equations (27)-(31) for secondary hair black hole.

 doi:10.20944/preprints202601.2185.v1

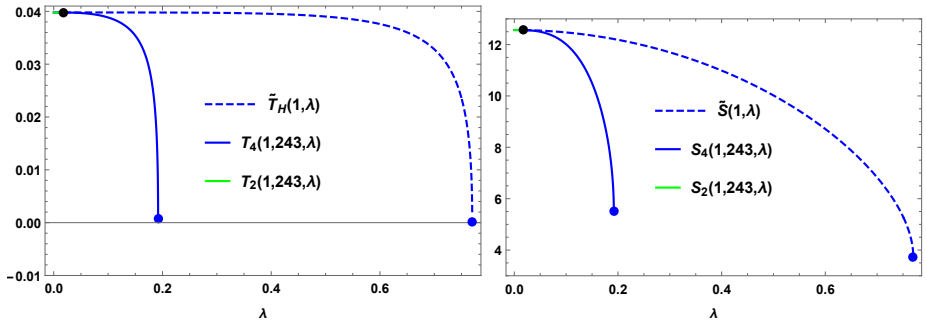

(**a**) (**b**)

Figure 3. Hawking temperature and entropy. (a) Four Hawking temperatures $T_2(1,243,\lambda)$ for $\lambda \in [0.0, 0.009]$, $T_4(1,243,\lambda)$ for $\lambda \in [0.009, 0.192]$ with $T_6(1,243,0.01746)$ (•), and $\tilde{T}_H(1,\lambda)$ for $\lambda \in [0, 0.7698]$. Two blue dots represent their extremal points at zero temperature. (b) Four entropies $S_2(1,243,\lambda)$ for $\lambda \in [0.0, 0.009]$, $S_4(1,243,\lambda)$ for $\lambda \in [0.009, 0.192]$ with $S_6(1,243,0.01746)$ (•), and $\tilde{S}(1,\lambda)$ for $\lambda \in [0, 0.7698]$.

3.1. Four Horizons

We separate four horizons from two double horizons because their thermodynamic properties are different. First of all, we observe allowed ranges for λ from Figure 2a: outer/inner horizons for primary hair black hole $r_{4/3}(M = 1, \xi = 243, \lambda \in [0.009, 0.192])$ with a point $r_6(1,243,0.01746) = 2$ (•) and extra horizons $r_{2/1}(1,243,\lambda \in [0, 0.009])$ forming a closed loop, and outer/inner horizons for secondary hair black hole $\tilde{r}_{\pm}(M = 1, \lambda \in [0, 0.7698])$. We note that the role of $r_2(1,243,\lambda)$ is an initially short connector to the outer horizon r_4. Figure 2b shows the largest loop formed by $r_{4/3}(1,34,\lambda \in [0.075, 0.379])$ and $r_{2/1}(1,34,\lambda \in [0, 0.075])$ with $r_6(1,34,0.125) = 1.288$ (•). Hereafter, we neglect r_1 and r_3 including $\tilde{r}_-$ for thermodynamic analysis because they represent inner horizons. Also, it is worthy to find that the existence region of $r_{4/3}(1,243,\lambda)$ for primary hair black hole is much narrower (a quarter) than $\tilde{r}_{\pm}(1,\lambda)$ of secondary hair black hole. Here, the outer boundaries of $\lambda = 0.192$ (•), 0.7698 (•) correspond to extremal black holes. Furthermore, it is known that the existence region of $\tilde{r}_{\pm}(1,\lambda)$ for secondary hair black hole is narrower than $\lambda \in [0, 1]$ of RN black hole with $M = 1$ and $Q = \lambda$. The above shows an apparent difference between primary, secondary hair (regular, Bardeen), and RN black holes.

Figure 3 indicates Hawking temperature and entropy as functions of λ. These thermodynamic quantities for primary hair black hole are narrower (a quarter) than those of secondary hair black hole, as predicted by r_4 and $\tilde{r}_+$. Also, it is clear that $S_4(1,243,\lambda) \leq \tilde{S}(1,\lambda)$ intrinsically for $\lambda \in [0.009, 0.192]$ because of $r_4 \leq \tilde{r}_+$. We find that two Hawking temperatures are zero at the extremal points $\lambda = 0.192$(•) and 0.7698(•). In addition, it is found that two Hawking temperatures are decreasing functions of M with different maxima, while two entropies are linearly increasing functions of M.

We note that the local (thermodynamic) stability condition is determined by positive heat capacity and the global (thermodynamic) stability condition provides us which one between two black holes is preferred [35]. It is given by the condition of $\Delta G < 0$. As is shown Figure 4a, heat capacity for primary hair black hole is defined properly for $\lambda \in [0.009, 0.192]$, but it blows up at $\lambda = 0.161$ (Davies point: •) and it is zero at $\lambda = 0.192$ (extremal point: •), while heat capacity for secondary hair black hole is well defined for $\lambda \in [0, 0.7698]$, but it blows up at $\lambda = 0.665$ (Davies point) and it is zero at $\lambda = 0.7698$ (extremal point). Here, it is clear that the Davies points [36] are not only critical points but also turning points indicating a change of thermal stability of the system.

 doi:10.20944/preprints202601.2185.v1

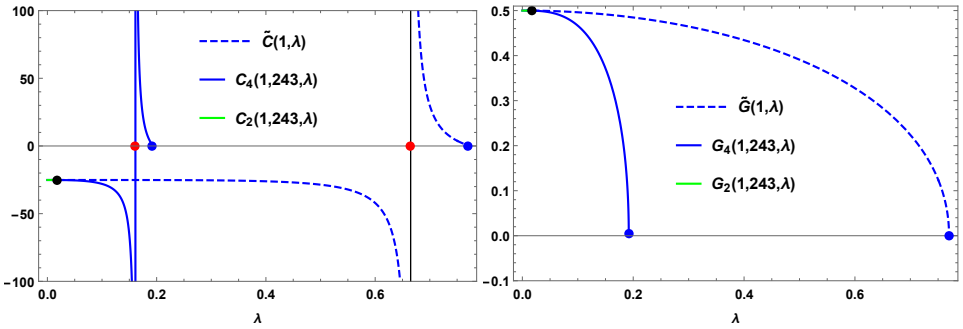

(a) (b)

Figure 4. Heat capacity and free energy. (a) Four heat capacities $C_2(1,243,\lambda)$ for $\lambda \in [0.0, 0.009]$, $C_4(1,243,\lambda)$ for $\lambda \in [0.009, 0.192]$ with $C_6(1,243,0.01746)$ (•), and $\tilde{C}(1,\lambda)$ for $\lambda \in [0, 0.7698]$. Two red dots (•) denote the Davies points and two blue dots (•) represent the extremal points. (b) Four free energies $G_2(1,243,\lambda)$ for $\lambda \in [0.0, 0.009]$, $G_4(1,243,\lambda)$ for $\lambda \in [0.009, 0.192]$ with $G_6(1,243,0.01746)$ (•), and $\tilde{G}(1,\lambda)$ for $\lambda \in [0, 0.7698]$. The blue dots (•) denote extremal points.

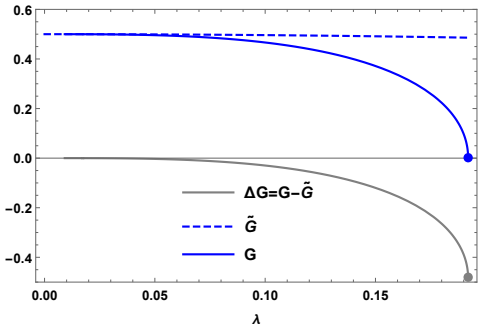

Figure 5. Difference for two free energies. $\Delta G(\lambda) \equiv G_4(1,243,\lambda) - \tilde{G}(1,\lambda) < 0$ for $\lambda \in [0.009, 0.192]$.

Figure 4b shows that Gibbs free energy for primary hair black hole is narrower (a quarter) than that of secondary hair black hole. We find that the Gibbs free energy for primary and secondary hair black hole are zero at the extremal point $\lambda = 0.192(\bullet)$ and $0.7698(\bullet)$.

Finally, it is interesting to mention a possibility of the phase transition between primary and secondary hair black holes. For this purpose, we propose the difference of two free energies in Figure 5. It is clear from Figure 4a that primary hair black hole is thermodynamically stable ($C_4 > 0$) for a short range of $\lambda \in [0.161(\bullet), 0.192(\bullet)]$, while secondary hair black hole is thermodynamically unstable ($\tilde{C} < 0$) for a long range of $\lambda \in [0, 0.665(\bullet)]$. Furthermore, the Gibbs free energy for primary hair black hole is less than that for secondary hair black hole for $\lambda \in [0.009, 0.192(\bullet)]$. This implies that a phase transition from secondary hair black hole to primary hair black hole is possible to occur for $\lambda \in [0.161(\bullet), 0.192(\bullet)]$.

3.2. Two Double Horizons

Concerning two double horizons, we choose two cases with $\xi = 5.51$ and 0.219. The first case shows its horizons and thermodynamics quantities in Figure 6. The major outer and inner horizons are described by $r_{2/1}(M = 1, \xi = 5.51, \lambda \in [0, 0.7697])$, forming a closed loop, whereas $r_{4/3}(M = 1, \xi = 5.51, \lambda \in [0.6972, 0.7697])$ cover the near-extremal secondary hair black hole partly. We note that the outer horizon has a discontinuity at $\lambda = 0.6972$, whose property propagates its thermodynamic quantities and shadow radius. Here, we wish to exclude $r_{4/3}$ because its thermodynamics mimics that of the near-extremal secondary hair black hole. The temperature is an increasing function of λ and its maximum is 306.2 at extremal point of $\lambda = 0.7697(\bullet)$. The entropy is a decreasing function of λ, its discontinuity occurs at $\lambda = 0.6972$, and it is zero at extremal point (•). The heat capacity has a Davies point (•) at $\lambda = 0.6384$, its discontinuity occurs near $\lambda = 0.6972$, and it is zero at extremal point (•).

 doi:10.20944/preprints202601.2185.v1

Finally, the Gibbs free energy is a decreasing function of λ and its zero is at extremal point ($\bullet$) (see Figure 6a).

For the case of $\xi = 0.219$, its outer/inner horizons $r_{2/1}(M = 1, \xi = 0.219, \lambda)$ are displayed in Figure 7a. They form a closed loop starting at $\lambda = 0$ and ending at $\lambda = 19.4$, contrasting to secondary hair black hole. Hence, its allowed λ-range is very wide like as [0,19.4], where the upper bound corresponds to the extremal point. One finds that two are separable until $\lambda = 5$, but they coincide nearly for $\lambda \in [5, 19.4]$. In this case, we mention that other horizons $[r_k(1, 0.219, \lambda)$, for $k = 3, \cdots, 8]$ are complex. It is very interesting to note that this solution could represent a feature of the black hole with primary scalar hair really because the scalarization usually enhances the allowed λ-range which is greater than the allowed λ for the bald black hole [19–21]. If Bardeen black hole is considered as a bald black hole, its allowed range is $\lambda \in [0, 0.7698]$ which is greater than $\lambda \in$[0,0.192] for four horizons with primary scalar hair. This may be unacceptable. But we have $\lambda \in [0, 19.4]$ for double horizons which is greater than that for Bardeen black hole. Its thermodynamic quantities are quite different from those for four horizons ($M = 1, \xi = 243, \lambda$) (see Figure 7b). Interestingly, we have an increasing temperature $T_2(1, 0.219, \lambda)$ and the entropy $S_2(1, 0.219, \lambda)$ for $\lambda \in [0.0, 19.4]$ whose upper bound corresponds to the extremal point. The former has a blow-up at the extremal point ($\bullet$), whereas the latter is a decreasing function of λ. The entropy at extremal point is zero. Also, we have the negatively increasing heat capacity $C_2(1, 0.219, \lambda)$ without Davies point but it is zero at the extremal point ($\lambda = 19.4$), while the free energy $G_2(1, 0.219, \lambda)$ is a decreasing function of $\lambda \in [0.0, 19.4]$ whose zero occurs at the extremal point. In this case, there is no counterpart to secondary hair black hole.

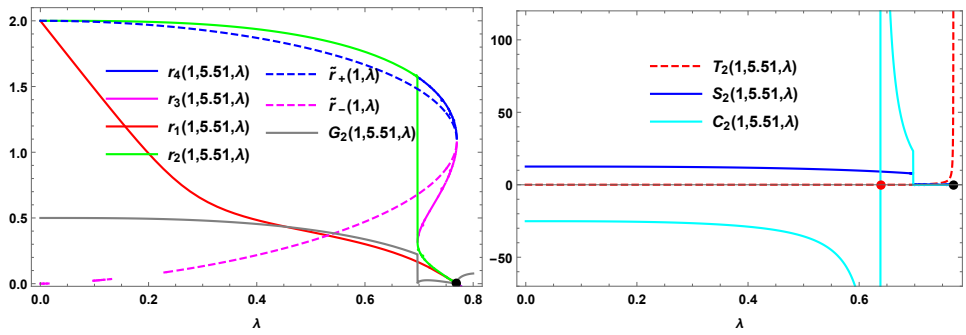

(**a**) (**b**)

Figure 6. (a) Outer/inner horizons $r_{2/1}(M = 1, \xi = 5.51, \lambda)$ as functions of $\lambda \in [0, 0.7697]$. In addition, two horizons $r_{4/3}(1, 5.51, \lambda)$ cover the near-extremal secondary hair black hole. Gibbs free energy $G_2(1, 5.51, \lambda)$ is displayed for $\lambda \in [0, 0.7697]$ whose upper bound denotes the extremal point($\bullet$). (b) Thermodynamic quantities: temperature $T_2(1, 5.51, \lambda)$, entropy $S_2(1, 5.51, \lambda)$, and heat capacity $C_2(1, 5.51, \lambda)$. The red dot ($\bullet$) denotes a Davies point at $\lambda = 0.6384$ and the black dot ($\bullet$) represents the extremal point at $\lambda = 0.7697$.

 doi:10.20944/preprints202601.2185.v1

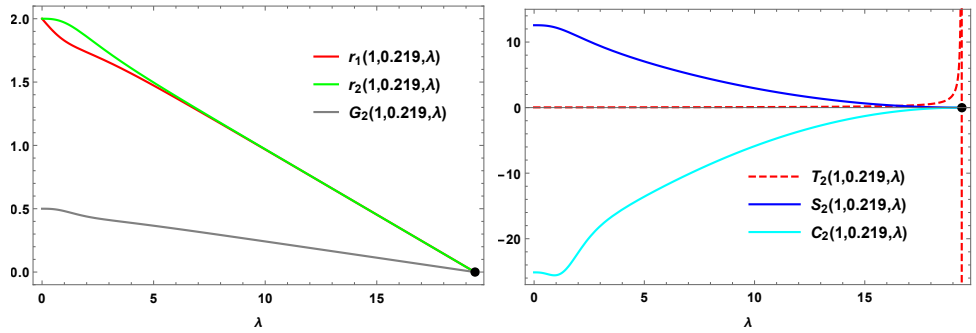

(a) (b)

Figure 7. (a) Outer/inner horizons $r_{2/1}(M = 1, \xi = 0.219, \lambda)$ as functions of $\lambda \in [0, 19.4]$ whose upper bound represents an extremal point (•). Gibbs free energy $G_2(1, 0.219, \lambda)$ is displayed for $\lambda \in [0, 19.4]$. (b) Thermodynamic quantities: temperature $T_2(1, 0.219, \lambda)$, entropy $S_2(1, 0.219, \lambda)$, heat capacity $C_2(1, 0.219, \lambda)$. The black dot (•) denotes an extremal point at $\lambda = 19.4$.

4. Shadow Radius Analysis

We analyzed thermodynamics of four and two double horizons where the four horizons is similar to the secondary hair (regular, Bardeen) black hole with difference in their allowed λ-ranges. Our next questions are: Which one is a better representation for black hole with primary scalar hair? What is the role of naked singularity (NS) found from two primary and secondary hair black holes? To answer, we need to analyze shadow radii by computing the critical impact parameter and compare them with the recent EHT observation. Requiring the photon sphere, one finds two conditions with potential $V(r) = h(r)/r^2$

$$V(r = L) = \frac{1}{2b^2}, \quad V'(r = L) = 0, \tag{36}$$

where b is the critical impact parameter and L represents the radius of unstable photon sphere. Equation (36) implies two relations

$$L_i^2 = h(L_i)b_i^2, \quad 2h(L_i) - L_i h'(L_i) = 0. \tag{37}$$

Here, two photon sphere radii and their critical impact parameters ($i = 2, 4$) are given by

$$L_i(M, \eta, \lambda, q), \tag{38}$$
$$b_i(M, \eta, \lambda, q), \tag{39}$$

whose explicit forms are too complicated to write down here. Similarly, we find photon sphere radius $\tilde{L}(1, \lambda)$ and its critical impact parameter $\tilde{b}(1, \lambda)$ for secondary hair black hole (S-branch) based on $f(r)$. We note that their NS-branches are arisen from the λ-extension of the photon spheres. However, there are no such NS-branches for two double horizons.

 doi:10.20944/preprints202601.2185.v1

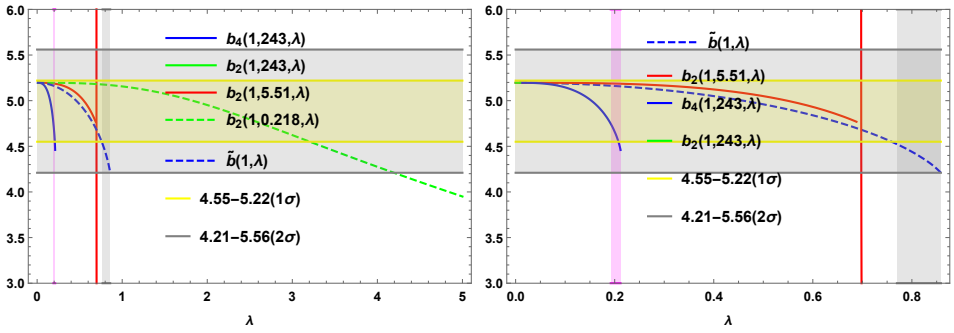

(a) (b)

Figure 8. (a) Five critical impact parameters $b_i(M=1,\xi=243,\lambda)$ for $i=2,4$, $b_2(1,5.51,\lambda)$, and $b_2(1,0.219,\lambda)$ with $\tilde{b}(1,\lambda)$ for secondary hair black hole (S) are as functions of $\lambda\in[0,5]$. There are two shaded regions $\lambda\in$[0.192,0.212] and [0.7698,0.8586] denoted by 4-NS and S-NS regions, respectively. Here, we introduce 1σ and 2σ ranges. (b) Enlarged critical impact parameters $b_4(1,243,\lambda)$, $b_2(1,5.51,\lambda)$, and $\tilde{b}(1,\lambda)$ are functions of $\lambda\in[0.0.8586]$. Two shaded columns include the 4-NS and S-NS branches. $b_2(1,5.51,\lambda)$ blows up at $\lambda=0.6972$.

Consulting the EHT observation (Keck- and VLTI-based estimates for SgrA$*$ [37–39]), the 1σ constraint on the shadow radius $r_{\rm sh}=b_i$ indicates [40]

$$4.55\lesssim r_{\rm sh}\lesssim 5.22 \tag{40}$$

and the 2σ constraint shows

$$4.21\lesssim r_{\rm sh}\lesssim 5.56. \tag{41}$$

Let us see Figure 8a for an explicit picture to test with the EHT observation. For the 2-branch with $\xi=0.219$, one has two constraints of the upper limit on its parameter λ: $\lambda\lesssim 3.21(1\sigma)$ and 4.19 (2σ), which is the new prediction from the double horizons surely. From Figure 8b, one observes that one narrow range of $0.009\lesssim\lambda\lesssim 0.21(1\sigma)$ exists for the 4 and 4-NS branches, while $\lambda\lesssim 0.759(1\sigma)$ and 0.858 (2σ) for S and S-NS branches. The former means that within 1σ, the 4 and 4-NS including an extremal point ($\lambda_{eP}=0.192$) are consistent with the EHT observation [40]. The latter implies that within 2σ, the S and S-NS including an extremal point ($\lambda_{eS}=0.7698$) are consistent with the EHT observation [40]. For the 2-branch with $\xi=5.51$, one has two constraints of the upper limit on its parameter λ: $\lambda\lesssim 0.6977(1\sigma)$ and $\lambda\lesssim 0.6978(2\sigma)$. Here, we observe that $b_2(1,5.51,\lambda)$ blows up near the discontinuity point ($\lambda=0.6972$) of $r_2(1,5.51,\lambda)$.

5. Discussions

We have investigated similarity and difference between primary (M,η,q,λ) and secondary (M,λ) hair black holes found in Beyond Horndeski gravity. We note that primary hair black hole has a complicated horizon structure seen from the metric function $h(r)$. In this study, (M,λ) play the major role of thermodynamic variables while $\xi=\eta q^5$ is used to choose three special cases of $\xi=243,5.51,0.219$ to describe primary hair black holes properly [30,31]. It is noted that the primary black hole is singular even though strong energy condition is violated for $r<\sqrt{2/3}\lambda$ and the secondary hair black hole is just the regular (Bardeen) black hole with mass M and magnetic charge λ obtained from the Einstein-nonlinear electrodynamics action. Furthermore, these two black holes violated no scalar-haired inner horizon theorem [22–25] because they have four and two double horizons.

First of all, we would like to mention the general feature on four horizons with $\xi=243$. We found that outer/inner horizons for primary hair black hole $r_{4/3}(M=1,\xi=243,\lambda\in[0.009,0.192])$ with a point $r_6(1,243,0.01746)=2$ (•), and extra horizons $r_{2/1}(1,243,\lambda\in[0,0.009])$ form a closed loop, while outer/inner horizons for secondary hair black hole are given by $\tilde{r}_\pm(M=1,\lambda\in[0,0.7698])$. For thermodynamic analysis, we neglected r_3,r_1, and $\tilde{r}_-$, while r_2 plays an initial connector to the outer horizon (r_4) simply. The existence region $\lambda\in[0.009,0.192]$ of primary black hole (r_4) is very narrower

 doi:10.20944/preprints202601.2185.v1

(a quarter) than that ($\lambda \in [0, 0.7698]$) for secondary hair black hole ($\tilde{r}_+$). The narrow existence region for λ propagates to defining all thermodynamic quantities of primary hair black holes.

However, we find that primary hair black hole is very similar to secondary hair black hole in the aspect of black hole thermodynamics. We have computed all thermodynamic quantities. Two black holes satisfy the same form for the first-law of thermodynamics and Smarr formula. There is a chance that the secondary hair black hole may transit into the primary hair black hole by analyzing Gibbs free energy and heat capacity. Our work would be meaningful because there is no consensus on the thermodynamics of the Bardeen black hole. The test for shadow radii implies that within 1σ, the 4 and 4-NS including an extremal point ($\lambda_{eP} = 0.192$) for primary hair black hole are consistent with the EHT observation, while within 2σ, the S and S-NS including an extremal point ($\lambda_{eS} = 0.7698$) for secondary hair black hole are consistent with the EHT observation [40]. The primary hair black hole possesses a better fit to EHT observation than secondary hair black hole.

To confirm a phase transition between primary and secondary hair black holes, one needs to clarify the stability of both primary and secondary hair black holes in Beyond Horndeski gravity. This may be other task. To this regard, one found that the $n = 0$ branch of scalarized charged black holes is stable against radial perturbations, while the Bardeen black hole without scalar hair is subject to tachyonic instability [18]. Here, a phase transition from the Bardeen black hole to the $n = 0$ branch of scalarized charged black holes is really possible to occur.

Concerning two double horizons $r_{2/1}(M = 1, \xi = 5.51 = 7, \lambda \in [0, 0.7697])$ and $r_{2/1}(M = 1, \xi = 0.219 = 7, \lambda \in [0, 19.4])$ for primary hair black holes, their thermodynamic properties are quite different from those for hour horizons. For $\xi = 5.51$, we note that the outer horizon $r_2(1, 5.51 = 7, \lambda)$ has a discontinuity at $\lambda = 0.6973$, whose property propagates its thermodynamic quantities and shadow radius. In addition, $r_{4/3}(1, 5.51, \lambda)$ survive and describe the near-extremal secondary hair black hole. Hence, this is considered as a mixture of ξ=243 and 0.219. The temperature is an increasing function of λ, the entropy is a decreasing function of λ, the heat capacity has a Davies point ($\bullet$) at $\lambda = 0.6384$, and the Gibbs free energy is a decreasing function of λ. In this case, one has two constraints of the upper limit on its parameter λ: $\lambda \lesssim 0.6977(1\sigma)$ and $\lambda \lesssim 0.6978(2\sigma)$ when testing it with EHT observation.

For $\xi = 0.219$, we obtained temperature $T_2(1, 0.219, \lambda)$ and entropy $S_2(1, 0.219, \lambda)$ where the former has a blow-up at the extremal point, whereas the latter is a decreasing function of λ. Also, we noted that the heat capacity $C_2(1, 0.219, \lambda)$ is an increasing function without Davies point but it has an extremal point at $\lambda = 19.4$, while the free energy $G_2(1, 0.219, \lambda)$ is a decreasing function of λ. We found that this has no counterpart to secondary hair black hole. For this 2-branch, one has two constraints of the upper limit on its parameter λ: $\lambda \lesssim 3.21(1\sigma)$ and 4.19 (2σ), which is considered surely as a new prediction from the double horizons of primary hair black hole.

Consequently, we described thermodynamics and shadow radius of primary hair black hole by choosing three special cases of $\xi(= \eta q^5) = 243, 5.51, 0.219$ and compared those with secondary hair (regular, Bardeen) black hole.

Acknowledgments: Y.S.M. is supported by the National Research Foundation of Korea (NRF) grant funded by the Korea government (MSIT) (RS-2022-NR069013).

References

1. Horndeski, G.W. Second-order scalar-tensor field equations in a four-dimensional space. *Int. J. Theor. Phys.* **1974**, *10*, 363–384. https://doi.org/10.1007/BF01807638.
2. Gleyzes, J.; Langlois, D.; Piazza, F.; Vernizzi, F. Healthy theories beyond Horndeski. *Phys. Rev. Lett.* **2015**, *114*, 211101, [arXiv:hep-th/1404.6495]. https://doi.org/10.1103/PhysRevLett.114.211101.
3. Crisostomi, M.; Hull, M.; Koyama, K.; Tasinato, G. Horndeski: Beyond, or not beyond? *JCAP* **2016**, *03*, 038, [arXiv:hep-th/1601.04658]. https://doi.org/10.1088/1475-7516/2016/03/038.
4. Kobayashi, T. Horndeski theory and beyond: A review. *Rept. Prog. Phys.* **2019**, *82*, 086901, [arXiv:gr-qc/1901.07183]. https://doi.org/10.1088/1361-6633/ab2429.
5. Langlois, D.; Noui, K. Degenerate higher derivative theories beyond Horndeski: Evading the Ostrogradski instability. *JCAP* **2016**, *02*, 034, [arXiv:gr-qc/1510.06930]. https://doi.org/10.1088/1475-7516/2016/02/034.

 doi:10.20944/preprints202601.2185.v1

6. Langlois, D. Degenerate Higher-Order Scalar-Tensor (DHOST) theories. In Proceedings of the 52nd Rencontres de Moriond on Gravitation, 2017, pp. 221–228, [arXiv:gr-qc/1707.03625].
7. Bakopoulos, A.; Charmousis, C.; Kanti, P.; Lecoeur, N. Compact objects of spherical symmetry in beyond Horndeski theories. *JHEP* **2022**, *08*, 055, [arXiv:gr-qc/2203.14595]. https://doi.org/10.1007/JHEP08(2022)055.
8. Kanti, P. Compact Objects in Einstein-scalar-Gauss-Bonnet Theory and beyond. In Proceedings of the 11th Aegean Summer School, 12 2024, [arXiv:gr-qc/2412.20296].
9. Babichev, E.; Charmousis, C. Dressing a black hole with a time-dependent Galileon. *JHEP* **2014**, *08*, 106, [arXiv:gr-qc/1312.3204]. https://doi.org/10.1007/JHEP08(2014)106.
10. Kobayashi, T.; Tanahashi, N. Exact black hole solutions in shift symmetric scalar–tensor theories. *PTEP* **2014**, *2014*, 073E02, [arXiv:gr-qc/1403.4364]. https://doi.org/10.1093/ptep/ptu096.
11. Babichev, E.; Charmousis, C.; Lehébel, A. Asymptotically flat black holes in Horndeski theory and beyond. *JCAP* **2017**, *04*, 027, [arXiv:gr-qc/1702.01938]. https://doi.org/10.1088/1475-7516/2017/04/027.
12. Bravo-Gaete, M.; Hassaine, M. Thermodynamics of a BTZ black hole solution with an Horndeski source. *Phys. Rev. D* **2014**, *90*, 024008, [arXiv:hep-th/1405.4935]. https://doi.org/10.1103/PhysRevD.90.024008.
13. Bakopoulos, A.; Charmousis, C.; Kanti, P.; Lecoeur, N.; Nakas, T. Black holes with primary scalar hair. *Phys. Rev. D* **2024**, *109*, 024032, [arXiv:gr-qc/2310.11919]. https://doi.org/10.1103/PhysRevD.109.024032.
14. Baake, O.; Cisterna, A.; Hassaine, M.; Hernandez-Vera, U. Endowing black holes with beyond-Horndeski primary hair: An exact solution framework for scalarizing in every dimension. *Phys. Rev. D* **2024**, *109*, 064024, [arXiv:hep-th/2312.05207]. https://doi.org/10.1103/PhysRevD.109.064024.
15. Bakopoulos, A.; Chatzifotis, N.; Nakas, T. Compact objects with primary hair in shift and parity symmetric beyond Horndeski gravities. *Phys. Rev. D* **2024**, *110*, 024044, [arXiv:gr-qc/2312.17198]. https://doi.org/10.1103/PhysRevD.110.024044.
16. Bakopoulos, A.; Chatzifotis, N.; Karakasis, T. Thermodynamics of black holes featuring primary scalar hair. *Phys. Rev. D* **2024**, *110*, L101502, [arXiv:hep-th/2404.07522]. https://doi.org/10.1103/PhysRevD.110.L101502.
17. Erices, C.; Fathi, M. Thermodynamic and observational constraints on black holes with primary hair in Beyond Horndeski gravity: Stability and shadows. *JCAP* **2025**, *01*, 016, [arXiv:gr-qc/2409.07312]. https://doi.org/10.1088/1475-7516/2025/01/016.
18. Zhang, L.; Pan, Q.; Myung, Y.S.; Zou, D.C. Spontaneous scalarization of Bardeen black holes. *Phys. Rev. D* **2024**, *110*, 124036, [arXiv:gr-qc/2409.11669]. https://doi.org/10.1103/PhysRevD.110.124036.
19. Herdeiro, C.A.R.; Radu, E.; Sanchis-Gual, N.; Font, J.A. Spontaneous Scalarization of Charged Black Holes. *Phys. Rev. Lett.* **2018**, *121*, 101102, [arXiv:gr-qc/1806.05190]. https://doi.org/10.1103/PhysRevLett.121.101102.
20. Myung, Y.S.; Zou, D.C. Instability of Reissner–Nordström black hole in Einstein-Maxwell-scalar theory. *Eur. Phys. J. C* **2019**, *79*, 273, [arXiv:gr-qc/1808.02609]. https://doi.org/10.1140/epjc/s10052-019-6792-6.
21. Myung, Y.S.; Zou, D.C. Quasinormal modes of scalarized black holes in the Einstein–Maxwell–Scalar theory. *Phys. Lett. B* **2019**, *790*, 400–407, [arXiv:gr-qc/1812.03604]. https://doi.org/10.1016/j.physletb.2019.01.046.
22. Cai, R.G.; Li, L.; Yang, R.Q. No Inner-Horizon Theorem for Black Holes with Charged Scalar Hairs. *JHEP* **2021**, *03*, 263, [arXiv:gr-qc/2009.05520]. https://doi.org/10.1007/JHEP03(2021)263.
23. Devecioglu, D.O.; Park, M.I. No scalar-haired Cauchy horizon theorem in Einstein-Maxwell-Horndeski theories. *Phys. Lett. B* **2022**, *829*, 137107, [arXiv:hep-th/2101.10116]. https://doi.org/10.1016/j.physletb.2022.137107.
24. An, Y.S.; Li, L.; Yang, F.G. No Cauchy horizon theorem for nonlinear electrodynamics black holes with charged scalar hairs. *Phys. Rev. D* **2021**, *104*, 024040, [arXiv:gr-qc/2106.01069]. https://doi.org/10.1103/PhysRevD.104.024040.
25. Dias, O.J.C.; Horowitz, G.T.; Santos, J.E. Inside an asymptotically flat hairy black hole. *JHEP* **2021**, *12*, 179, [arXiv:hep-th/2110.06225]. https://doi.org/10.1007/JHEP12(2021)179.
26. Rodrigues, M.E.; de Sousa Silva, M.V. Bardeen Regular Black Hole With an Electric Source. *JCAP* **2018**, *06*, 025, [arXiv:gr-qc/1802.05095]. https://doi.org/10.1088/1475-7516/2018/06/025.
27. Ayon-Beato, E.; Garcia, A. Regular black hole in general relativity coupled to nonlinear electrodynamics. *Phys. Rev. Lett.* **1998**, *80*, 5056–5059, [gr-qc/9911046]. https://doi.org/10.1103/PhysRevLett.80.5056.
28. Ayon-Beato, E.; Garcia, A. The Bardeen model as a nonlinear magnetic monopole. *Phys. Lett. B* **2000**, *493*, 149–152, [gr-qc/0009077]. https://doi.org/10.1016/S0370-2693(00)01125-4.

 doi:10.20944/preprints202601.2185.v1

29. Myung, Y.S.; Nakas, T. Smarr formula for black holes with primary and secondary scalar hair. *Phys. Rev. D* **2025**, *112*, 064002, [arXiv:gr-qc/2505.02368]. https://doi.org/10.1103/qv3n-r8q9.
30. Zhang, Y.; Gao, S. First law and Smarr formula of black hole mechanics in nonlinear gauge theories. *Class. Quant. Grav.* **2018**, *35*, 145007, [arXiv:gr-qc/1610.01237]. https://doi.org/10.1088/1361-6382/aac9d4.
31. Hajian, K.; Tekin, B. Coupling Constants as Conserved Charges in Black Hole Thermodynamics. *Phys. Rev. Lett.* **2024**, *132*, 191401, [arXiv:gr-qc/2309.07634]. https://doi.org/10.1103/PhysRevLett.132.191401.
32. Quevedo, H.; Quevedo, M.N.; Sanchez, A. Thermodynamics and geometrothermodynamics of regular black holes **2024**. [arXiv:gr-qc/2405.04474].
33. Merriam, A.; Sarwar, M.Z. Thermodynamics of Bardeen regular black hole with generalized uncertainty principle. *Int. J. Mod. Phys. D* **2022**, *31*, 2150128, [arXiv:gr-qc/2110.11011]. https://doi.org/10.1142/S0218271821501285.
34. Wang, Z.; Ren, H.; Chen, J.; Wang, Y. Thermodynamics and phase transition of Bardeen black hole via Rényi statistics in grand canonical ensemble and canonical ensemble. *Eur. Phys. J. C* **2023**, *83*, 527. https://doi.org/10.1140/epjc/s10052-023-11680-y.
35. Anusonthi, T.; Wongjun, P.; Nakarachinda, R. Thermodynamic Stability of Schwarzschild-de Sitter Black holes with Rényi entropy. *J. Phys. Conf. Ser.* **2025**, *2934*, 012011, [arXiv:gr-qc/2501.04378]. https://doi.org/10.1088/1742-6596/2934/1/012011.
36. Davies, P.C.W. Thermodynamics of black holes. *Rept. Prog. Phys.* **1978**, *41*, 1313–1355. https://doi.org/10.1088/0034-4885/41/8/004.
37. Akiyama, K.; et al. First Sagittarius A* Event Horizon Telescope Results. I. The Shadow of the Supermassive Black Hole in the Center of the Milky Way. *Astrophys. J. Lett.* **2022**, *930*, L12, [arXiv:astro-ph.HE/2311.08680]. https://doi.org/10.3847/2041-8213/ac6674.
38. Akiyama, K.; et al. First Sagittarius A* Event Horizon Telescope Results. III. Imaging of the Galactic Center Supermassive Black Hole. *Astrophys. J. Lett.* **2022**, *930*, L14, [arXiv:astro-ph.HE/2311.09479]. https://doi.org/10.3847/2041-8213/ac6429.
39. Akiyama, K.; et al. First Sagittarius A* Event Horizon Telescope Results. VI. Testing the Black Hole Metric. *Astrophys. J. Lett.* **2022**, *930*, L17, [arXiv:astro-ph.HE/2311.09484]. https://doi.org/10.3847/2041-8213/ac6756.
40. Vagnozzi, S.; et al. Horizon-scale tests of gravity theories and fundamental physics from the Event Horizon Telescope image of Sagittarius A. *Class. Quant. Grav.* **2023**, *40*, 165007, [arXiv:gr-qc/2205.07787]. https://doi.org/10.1088/1361-6382/acd97b.